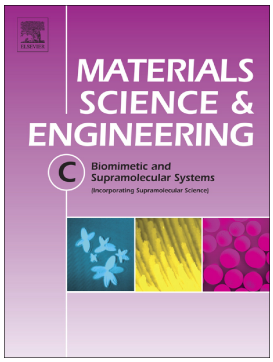

Enhanced bioactivity of a rapidly-dried sol-gel derived quaternary bioglass

Basam A.E. Ben-Arfa, Isabel M. Miranda Salvado, José M.F. Ferreira, Robert C. Pullar

PII: S0928-4931(17)33964-4
DOI: doi:10.1016/j.msec.2018.05.016
Reference: MSC 8571

To appear in: *Materials Science & Engineering C*

Received date: 2 October 2017
Revised date: 21 March 2018
Accepted date: 3 May 2018

Please cite this article as: Basam A.E. Ben-Arfa, Isabel M. Miranda Salvado, José M.F. Ferreira, Robert C. Pullar , Enhanced bioactivity of a rapidly-dried sol-gel derived quaternary bioglass. The address for the corresponding author was captured as affiliation for all authors. Please check if appropriate. Msc(2017), doi:10.1016/j.msec.2018.05.016

Enhanced bioactivity of a rapidly-dried sol-gel derived quaternary bioglass

Basam A. E. Ben-Arfa, Isabel M. Miranda Salvado*, José M. F. Ferreira and Robert C. Pullar*

Department of Materials and Ceramic Engineering / CICECO – Aveiro Institute of Materials, University of Aveiro, 3810-193 Aveiro, Portugal

Abstract

Novel quaternary (67Si-24Ca-10Na-8P) glass powders were successfully synthesised by sol-gel followed by two alternative drying schedules, conventional drying (CD) and an innovative fast drying (FD) process (200 times quicker). The glasses were thermally stabilised at 550 ºC, and then characterised by different complementary techniques. The samples showed very similar silica network structures, with the FD one having slightly lower degree of polymerisation than the CD sample. This less polymerised, more open, network structure exhibited an improved bioactivity in simulated body fluid (SBF), probably also due to the apparent presence of poorly crystalline HAp in the stabilised glass powder. In contrast, the CD glass exhibited an unwanted secondary crystalline silica phase. Both glasses showed excellent biomineralisation upon immersion in SBF, being more pronounced in the case of FD with clear evidence of HAp formation after 4 h, while equivalent signs in the CD samples were only noticed after longer immersion periods between 8 h and 1 week.

Keywords: Glass; Glass-ceramics; Crystallisation; Bioactivity; Hydroxyapatite

*To whom correspondence should be addressed:
E-mail: isabelmsalvado@ua.pt, rpullar@ua.pt

1. Introduction

Glasses find applications in many modern technologies and industries **[1]**. These materials can be prepared by the traditional melting route or via sol-gel **[2]**. Sol-gel offers several advantages, including an atomic level mixing of the batch components at room temperature (RT), lower processing temperatures **[3]** that prevent preferential volatilisation of certain components, and an enhanced homogeneity of the glasses **[4]**. This synthesis route attracted increasing attention from the research community after the first sol-gel preparation of a multicomponent glass in 1950 **[2]**, being considered a promising technique for producing bioactive glasses and glass ceramics. The high surface area of sol-gel derived materials, the presence of micro pores and of residual hydroxyl ions confer them enhanced bioactivity **[1]**. However, a long aging processing step is usually required to harden the sol network **[4]**, which affects the final microstructure and the mineralisation ability of sol-gel bioglasses **[5]**. Increasing aging times are often accompanied by a noticeable decreases in bioactivity **[4]**. Therefore, the aim of this work is to improve the bioactivity of a four-component bioglass and overcoming the problem of long aging stages in sol-gel processing by following a new rapid sol-gel synthesis method developed by the authors **[6]**. This rapid approach uses a rotary evaporator to dry the sol to a near amorphous bioglass gel in 1 h and has been already tested for bioglasses with Ca and P contents equivalent to stoichiometric hydroxyapatite (HAp, Ca/P = 1.67) **[7]**.

Typical examples of bioactive glasses in quaternary systems are 45S5 and S53P4. 45S5 is probably the most well-known bioactive glass, containing 26.9 mol% CaO and with Ca/P ~5 **[8]**, while S53P4 is another famous bioactive glass with 20 mol% CaO and Ca/P = 5 **[9]**. The most common sol-gel bioactive glasses in this ternary system are 58S, which contains 36 mol% CaO and Ca/P = 4.5 **[10]**, and 77S with 16 mol% CaO and Ca/P = 2 **[11]**.

In terms of network structure, melt derived 45S5 bioglass consists of 69% chains and rings of Q^2, with 31% of Q^3 units providing some cross-linking **[12]**. It has been suggested that bioglasses with network connectivity (N_c) greater than 2.6 lack bioactivity **[13]**. However, sol-gel glasses often do not obey the N_c calculations, as H^+ can also be considered as a network modifier, which increases the glass's dissolution rate **[14]**.

In the present work, a quaternary bioglass composition enriched in calcium (Ca/P = 3: $67SiO_2 - 5Na_2O - 24CaO - 4P_2O_5$) was selected to investigate the effect of a larger amount of modifier on the network structure and HAp formation *in vitro*. The high silica content is justified by its role as primary nucleation centre for apatite formation **[15]** and to foster mechanical strength. The content of phosphate was kept intentionally low as its role in the glass is only to aid the nucleation of calcium phosphate **[16]**. The presence of Na_2O (5 mol%) in the glass compositions aims at enhancing the degradation rate **[17]**, stimulate bone formation and differentiation **[18,19]**, and the apatite-forming ability *in-vitro* **[19]**.

2. Materials and methods

2.1 Glass synthesis

Tetra-ethyl-*ortho*-silicate (TEOS, $C_8H_{20}O_4Si$, 98%), calcium nitrate tetrahydrate (CaN, $Ca(NO_3)_2.4H_2O$, ≥ 99%), sodium nitrate (NaN, $NaNO_3$, ≥ 99%) and triethyl phosphate (TEP, $C_6H_{15}O_4P$, ≥ 99.8%) were used as precursors for silica, calcium oxide, sodium oxide and phosphorus oxide, respectively. All four precursors were supplied from Sigma-Aldrich. Distilled water was used as solvent and citric acid monohydrate (CA, $C_6H_8O_7.H_2O$, 99.5–102%, Sigma-Aldrich) was added to catalyse the sol-gel hydration and polymerisation reactions.

The four-component composition was selected in the (Si–Na–Ca–P) system: $67SiO_2 - 5Na_2O - 24CaO - 4P_2O_5$ (mol %, Ca/P = 3), as shown in **Table 1**.

20 mL of 0.15 M aqueous solution of CA was poured in 150 ml glass beaker, and 24 ml TEOS and 2.2 mL TEP were sequentially added quickly to this solution. After a clear sol was formed, 1.3616 g of NaN was dissolved separately in 10 mL 0.15 M aqueous solution of CA, stirred for 10 min, and then added quickly to the beaker containing the TEOS and TEP. 9.0798 g of CaN was dissolved separately in 50 mL 0.15 M aqueous solution of CA and added quickly to the beaker containing the other three components. This solution was then stirred for 1 h at RT as schematised the flow chart diagram of **Fig. 1**. The resulting sol was divided into two equal parts. One half was poured into a glass petri dish (120 mm diameter, 20 mm high) to be aged and dried by conventional drying (CD). The sample was aged at RT for 4 h, followed by drying in an oven at 35°C/3 days, then at 50°C/6 days, and finally at 100°C/3 days, making a total of 12 days (288 h) **[19]** for the sample **67S24C–CD**.

The second half was rapidly dried in a rotary evaporator Buchi 210 Rotavapor with V-850 vacuum controller and V-700 diaphragm vacuum pump (Buchi Labortechnik AG, Flawil, Switzerland). The sols were dried in a 500 mL pear-shaped flask while rotating in a water bath at 55°C and under a pressure of 50 mbar for 1 h **[19]**. This drying process was 288 times quicker and the as obtained sample was designated as **67S24C–FD** (with FD standing for fast drying). Both processes are summarised in **Fig. 1** and **Table 1**.

Both dried gels were thermally stabilised at 550°C in air for 1 h. The heating rate was 1°C/min up to 300°C for 1 h, and then increased to 10°C/min up to 550°C, holding for 1 h at this temperature, followed by natural cooling. The heat-treated samples were ground using a mortar and pestle to obtain glass powders, which were sieved through a 40–63 micron mesh and then used for all the subsequent characterisations.

2.2 Glass characterisation

The specific surface areas (SSA) of the powders were estimated using the Brunauer-Emmett-Teller (BET) method using a Gemini M-2380 (Micrometrics, Norcross, GA) with N_2 as the adsorbate. Samples were degassed at 200 °C before performing the analysis.

Skeletal density was determined by helium pycnometry. The particle size was measured using a laser diffraction particle size analyser (Coulter LS particle size analyser; Beckman Coulter, CA).

The crystalline phase analysis of the samples before and after immersion in simulated body fluid (SBF) was performed by X-ray diffraction (XRD, PANalytical XPERT-PRO Diffractometer system), using Cu Kα radiation (Kα =1.54059 Å) with 2θ varying from 6−70º in steps of 0.026 s^{-1}. The diffraction patterns were compared with JCPDS standards **[20,21]**.

The ^{29}Si MAS-NMR spectra were recorded in a ASX 400 spectrometer (Brucker, Germany) operating at 79.52 MHz (9.4 T), using a 7 mm probe at a spinning rate of 5 kHz. The pulse length was 2 µs with 60 s delay time. The aim was to investigate the silica environments and the degree of silica polymerisation of the stabilised glass samples. Kaolinite was used as a chemical shift reference. ^{29}Si MAS NMR spectra were deconvoluted using dimFit software.

Infrared transmittance spectra of the glasses, before and after immersion in SBF, were obtained using a Fourier Transform Infrared Spectrometer (FTIR, Tensor 27, Brucker, Germany) in the range of 350−4000 cm^{-1}, with 128 Scans and 4 cm^{-1} resolution. The pellets were prepared by pressing a mixture of KBr and glass powder with ratio of 1/150 (by weight) and pressed into a pellet using a hand press.

2.3 Bioactivity tests

The *in-vitro* bioactivity in simulated body fluid (SBF) was assessed by immersion of 75 mg of glass powders from samples in 50 mL of SBF solution at 37 ºC following a unified approach recommended elsewhere **[22]**. The ionic concentrations of the SBF (in mmol L^{-1}: Na^+ = 142.0, K^+ = 5.0, Ca^{2+} = 2.5, Mg^{2+} = 1.5, CI^- = 125.0, HPO_4^{2-} = 1.0, HCO_3^- = 27.0 and SO_4^{2-} = 0.5) are virtually equivalent to those of human plasma **[23]**. The powder–SBF mixtures were immediately sealed into plastic flasks and placed in an incubator at 37 ± 0.5 ºC on an orbital shaker set at 120 rpm. The sampling took place for 7 different times: (4 h, 8 h, 72 h, 1 week, 2 weeks, 3 weeks and 4 weeks) **[22]**. At the end of each time period, the sample was removed from the incubator and the solids were collected by centrifuging the mixture at 10,000 rpm under vacuum for 30 min, using a Beckman model LB-70M ultracentrifuge. The pH of the separated solution was measured directly, while the separated particles were washed with deionised water and subsequently with acetone to terminate the reaction, and after separation for the second time, dried in an oven overnight at 37 ºC. The experiments were performed in triplicate in order to ensure the accuracy of results. The apatite-forming ability of the glass powders was followed by XRD, FTIR, and SEM analysis, and pH measurement.

3. Results and discussion

3.1 Surface area and density measurements

Table 2 shows the data of density, particle size and specific surface area measured for the thermally stabilised glass powders obtained by the two drying schedules. As can be seen, the protocol used for drying and aging drastically affects the physical properties of the resulting materials. The density of **67S24C–CD** is only slightly lower in comparison to

that of **67S24C–FD**, but the SSA of **67S24C–CD** glass powder is more than 1.4 times greater than that of **67S24C–FD** sample. The higher SSA value of **67S24C–CD** can be attributed to the fine porous network formed during the long and undisturbed sol-gel transition followed by solvent evaporation from the pores. The impacts on the *in vitro* bioactivity will depend not only on the extent of surface area exposed to SBF but also on the degree of glass network connectivity and how it is affected by the drying schedule, as will be discussed below.

3.2 Structure of the stabilised glasses

3.2.1 MAS-NMR analysis

The measured and deconvoluted ^{29}Si MAS NMR spectra for **67S24C–FD** and **67S24C–CD** routes are shown in **Fig. 2**. Deconvolution enabled identifying the various Q^n species, where *n* denotes the number of bridging oxygens and can assume the values of 1, 2, 3 or 4. The condensation degree (D_c) values calculated by using the Equation 1 below **[24]** are presented in **Table 3**.

$$D_c = \frac{1\times Q^1 + 2\times Q^2 + 3\times Q^3 + 4\times Q^4}{4} \times 100\% \qquad (1)$$

The network connectivity N_c can be calculated from the % integral of Q^n acquired from the NMR deconvolution by dimFit using Equation 2 **[25]**:

$$Nc = 4\left(\frac{Q^4}{100}\right) + 3\left(\frac{Q^3}{100}\right) + 2\left(\frac{Q^2}{100}\right) + 1\left(\frac{Q^1}{100}\right) \qquad (2)$$

The chemical shifts at ~ –100.2 and ~ –100.7 ppm are assigned to Q^3 species for **67S24C–FD** and **67S24C–CD** samples, respectively, while Q^4 species are observed around –110 ppm for the two glasses. Both glasses also contain significant populations of Q^2 and Q^1 species as well, between –94.4 to –96.4 ppm, and –86.5 and –88.2 ppm, respectively (**Table 3**). Although the two samples have the same composition, the proportions of the Q^n

species are significantly different. **67S24C–FD** has fewer Q^4 species than **67S24C–CD**, but a greater number of Q^2 and Q^1 species, with the difference of ~10% in Q^2 species between the FD and CD routes being particularly significant. **67S24C–FD** also has consistently lower chemical shift values as a result of less extensive polymerisation. This means that **67S24C–FD** has a smaller D_c value (71.8 %) than **67S24C–CD** (78.4%), which also translates in lower calculated network connectivity (N_c =3.0) for **67S24C–FD** in comparison to **67S24C–CD** (N_c =3.2). These results are shown in **Table 3**. Different drying protocols for the same proportions of modifiers results in different extents of silica network disruption. The **67S24C–FD** sample exhibits a lower degree of network connectivity compared with **67S24C–CD** and is likely to be more readily mineralised upon immersion in SBF. This result is consistent with our previous observations made for FD bioglasses of the same Si–Ca–Na–P system but containing lower amounts of Ca modifier bioglasses with Si/Ca ratios of 76/10 **[26]** and 76/9 **[7,26]**. These CD bioglasses only showed Q^4 and Q^3 silica species; with ~70-75% being fully connected Q^4. The FD method produced glasses with a slightly lower degree of connectivity (D_c = 91.8% for FD *vs.* 93.8% for CD) **[16]**. Moreover, all these glasses with lower contents of Ca modifier exhibited greater extents of network connectivity (N_c = ~3.7) than the present calcium-rich bioglasses with a Si/Ca ratio of 67/24 (approximately 3 times less than in refs **[7,26]**). The higher amount of modifier used in this work resulted in a much less polymerised glass network structure, which is expected to have positive impacts on its *in vitro* bioactivity in SBF.

3.2.2 X-ray diffraction (XRD)

Fig. 3a shows the XRD patterns of the stabilised glasses. Both have some traces of crystallinity in a highly amorphous glass matrix, but it is apparent that **67S24C–FD** is less

crystalline than **67S24C–CD**. This result is in a good agreement with our previous findings for a different glass system showing that the FD method could to some extent suppress crystallisation **[26]**. **67S24C–CD** contains crystalline silica (coesite SiO_2, PDF card #04-015-7166) **[20]**. This phase was not formed in FD sample, a feature that favours the **67S24C–FD** process. A very poorly crystalline HAp [$Ca_{10.12}(H_{1.26}P_{5.99}O_{23.88})(OH)_{2.05}$, PDF card #01-080-3956] **[21]** is a common secondary phase in both samples. The corresponding broad XRD peaks suggest that crystals are at nanoscale, which may act as seeds for the crystallisation for HAp formation and growth upon immersion in SBF.

In our previous compositions **[7,26]** with Ca/P ratios corresponding to stoichiometric HAp (Ca/P = 1.67) and tri-calcium phosphate (TCP, Ca/P = 1.5), the stabilised glasses never exhibited the formation of crystalline HAp. Instead, the crystalline phases observed in both FD and CD produced glasses were $NaCa(PO_4)$ **[26]** and $CaNa_4Si_3O_9$ **[7]**. Therefore, it seems that the much higher ratio of Ca/P used here (Ca/P = 3) enables squeezing sufficient calcium from the glass network to form nanocrystalline HAp. This should also assist the formation and growth of HAp from these bioglasses in body fluids. Further manipulation of the Ca/P ratio in the glass composition may enable control over the exact calcium phosphate phase which can be crystallised **[27]**.

3.2.3 FTIR spectra

The FTIR spectra of the two stabilised glasses are presented in **Fig. 3b**. They are typically dominated by a broad band between 900 and 1300 cm^{-1}, assigned to asymmetric stretching for Si–O–Si centred at ~1080 cm^{-1} **[28]**, which represents the transverse optical (TO_1) Si–O–Si stretching mode. Moreover, a shoulder at ~1225 cm^{-1} represents the Si–O–Si (TO_2) stretching mode **[29]**, as a result of the introduction of P_2O_5 into silica glass **[30]**. The longitudinal optical (LO) vibration can be observed at 1170 cm^{-1} **[31]**. The very faint

bands around 880 cm^{-1} and 1425–1460 cm^{-1} are assigned to C–O bonds (probably small amounts of carbonate) **[24,32,33]**. The main signal in **67S24C–CD** is divided into two peaks; one appears at 1092 cm^{-1} and the other at 1045 cm^{-1}. These peaks, along with the with the two shoulders at 1170 cm^{-1} and 1225 cm^{-1}, are assigned to Si–O stretching modes for tetrahedral coesite (a less common form of SiO_2), and the 796 cm^{-1} peak is also assigned to Si–O–Si stretching frequencies of various silica phases, including coesite **[27,28]**. This splitting is much less apparent in FD suggesting it may not contain the coesite phase, but instead quartz with a peak at 1080 cm^{-1}.

The appearance of the twin peaks at ~570 and ~ 603 cm^{-1} for the two glasses can be attributed to phosphate group PO_4^{3-}, being usually considered an evidence for the presence of HAp. The other characteristic phosphate peaks for HAp appear at around 962, 1034 and 1092 cm^{-1} **[34]** and considering their low intensities, they are probably masked by the strong and broad silica peaks in these glasses. Representative HAp peaks were not observed in our previously reported stabilised glasses with stoichiometric Ca/P ratios corresponding to HAp and TCP **[7,26]**. Bands characteristic of (COO^-) group, maybe from the catalyst citric acid species, can be seen as twin peaks at 1540 cm^{-1} and at 1571 cm^{-1}, assigned respectively to $\upsilon_{as}(COO^-)$ and $\upsilon_s(COO^-)$ vibration modes **[35]**. The peak observed at ~1635 cm^{-1} can be assigned to the bending vibration of molecular water **[36]**.

3.2.4 Scanning Electron Microscope (SEM) images

The SEM images of the stabilised glasses are sown in **Fig. 3c**. It can be seen that both glass powders consist of agglomerated primary nanoparticles (NPs) with approximate dimensions of 30–50 nm. These approximately spherical NPs associate to form submitter agglomerates. No significant morphological differences can be observed between **67S24C–FD** and **67S24C–CD** samples. Their appearances resemble the morphologies observed for

the corresponding stabilised glass powders prepared by the same FD and CD routes reported previously by the authors **[7,26]**.

3.3 Bioactivity assessment

3.3.1 XRD after immersion in simulated body fluid (SBF)

Fig. 4a displays the XRD patterns of the **67S24C–FD** and **67S24C–CD** samples, respectively, after immersion in SBF for different periods of time up to 4 weeks. The crystalline SiO_2 phase seen in CD (Coesite, PDF card #04-015-7166) has apparently disappeared, being probably hidden by the poorly-crystalline HAp surface layer. This hypothesis is consistent with the observed gradual intensification of the HAp peaks (PDF # 01-080-3956) already identified in the stabilised glasses. There major changes in the degree of crystallinity were observed between 4 h and 4 weeks of immersion. Within the period from 72 h to 4 weeks, **67S24C–FD** with sharper and better defined major peaks seems to have undergone a slightly more extensive biomineralization process in comparison to **67S24C–CD**. This supports the hypothesis that the FD method fosters the *in vitro* bioactivity (the ability to deposit a surface layer of HAp), attributed to the less polymerized silica network structure of **67S24C–FD** (50.3% Q^4, 29.0% Q^2) in comparison to **67S24C–CD** (62.3% Q^4, 19.4% Q^2).

The earlier tested bioglass powders with Ca/P ratios corresponding to stoichiometric HAp and TCP phases did not show the formation of crystalline HAp until after 3–4 weeks of immersion in SBF, and even then, only for the powder with Ca/P = 1.67 and under shaking at 120 RPM **[7]**.

3.3.2 FTIR spectra after immersion in SBF

Fig. 4b shows the evolution of the FTIR bands upon immersion in SBF over different time periods. The major HAp band at around 1034 cm^{-1} is still masked by the large silica band, but the two characteristic phosphate peaks of HAp at around 560 and 600 cm^{-1} are clearly present and sharp after just 4 h of immersion for both samples, and the weak-but-sharp 962 cm^{-1} peak is faintly visible **[37]**. This may confirm the dissolution of HAp and the evolution of a new HAp phase, as suggested by XRD. As observed by XRD, there are little changes over time with HAp peaks becoming better defined and sharper after 72 h, with the changes being slightly more noticeable for **67S24C–FD** than for **67S24C–CD** between 72 h and 4 weeks. The FTIR data also support the superior bioactivity of the present composition and of the FD method in comparison the lower Ca/P ratio and CD reported in our previous studies **[7]**. Here, the presence of existing HAp NPs in the stabilised powders and the less polymerised network structure seem to be the reasons for the enhanced bioactivity.

The two tiny non-HAp related peaks at 1425–1460 cm^{-1} were replaced by wide band centred at ~1450 cm^{-1}, which is assigned to the C–O group. Also the evolution of the peak at 880 cm^{-1} evidences the presence of carbonated hydroxyapatite formation (CHAp). It can be classified as type A due to the band being centred at 1450 cm^{-1} and the peak at 880 cm^{-1} **[34,38]**. The band at 1045 cm^{-1} belongs to a more linear silica structure. The shifting of the main bands from 1080–1092 to 1100 cm^{-1} for the two glass samples could also be attributed to transformation of the silica structure to a less cross linked and more linear structure due to SBF immersion **[39]**. The appearance of a new band at ~960 cm^{-1} could be assigned to stretching vibrational mode of Si–OH **[40–42]**, although as stated above there is a weak HAp peak at 962 cm^{-1}, and it is also reported that a peak at about 960 cm^{-1}

could be assigned to P–O symmetric stretching in the formed layer of CHAp layer on the powder surface **[43]**. This may show the occurrence of the 5 stages of hydroxycarbonated apatite (HCA) layer formation as proposed by Hench *et al.* **[43]** during the initial hours of immersion in SBF. Although the FTIR spectra of both glasses are very similar, after 72 h **67S24C–FD** shows sharper and better defined peaks supporting its enhanced bioactivity in comparison to **67S24C–CD**. Interestingly, sharpness of FTIR HAp peaks can only be noticed after 4 h in the **67S24C–CD** sample.

The morphological evolution of the HAp layer deposited onto the surface of **67S24C–FD** and **67S24C–CD** along the immersion time in SBF is shown in the SEM images displayed in **Fig. 6**. A network of poorly crystalline platy flakes has been deposited after only 4h for both glasses, with relatively higher deposition of HAp on the surface of **67S24C–CD** as shown in **Fig. 6a**. After 8 h of SBF immersion **Fig. 6b**, HAp deposition increased intensively in both glasses, maintaining a higher bioactivity for **67S24C–CD**, with a denser HAp deposited layer. At 1 week, **Fig. 6c**, it can be observed that the higher bioactivity favours the **67S24C–FD** glass, as shown by highly uniform layer covering the glass surface. The bioactivity exhibits similar behaviour after 4 w of SBF immersion with almost similar morphology, as can be seen in **Fig. 6d**.

3.3.3 pH behaviour in SBF

The pH variations along the immersion time in SBF for the **67S24C–FD** and **67S24C–CD** samples exhibit almost identical trends as shown in **Fig. 5**. The pH variations for both samples run in parallel within the 7.40–7.75 range, being slightly smaller for **67S24C-FD**. A rapid initial increase in pH values from the starting value of 7.4 was registered for both samples after just 4 h, attributed to the leaching of alkaline Na and alkaline earth Ca from the surface of the glass particles. This increasing step is then

followed by a gradual reversal trend starting between 4 h to 8 h, which might be due to the partial dissolution of acidic glass former species such as Si^{4+} and phosphate ions; and to the precipitation of HAp, as confirmed by XRD and FTIR spectra. The two samples then underwent a gradual increase in pH reaching plateaux values within 3–14 days, followed by slow general decreasing trends with the accomplishment of the surface HAp coating layer. Seemingly, the *in vitro* biomineralisation occurred through three-stages: (i) initial fast ionic exchanges, saturation of the SBF solution and surface precipitation of poorly crystalline HAp (4–8 h); (ii) the continuation of the dissolution-precipitation reactions but at a slower pace (3–14 days); followed by (iii) a trend towards stabilization due to the gradual depletion of Ca and P species in the SBF solution and the completeness of the surface HAp coating layer. The observed pH changes are consistent with the previous results obtained by XRD and FTIR.

3.3.4 SEM images after immersion in SBF

The SEM micrographs of the **67S24C-FD** and **67S24C-CD** samples immersed in SBF for different time periods (4 h, and 4 w) are shown in (**Fig. 6a-b)**. After just 4 h the microstructure has already evolved significantly from that observed before immersion in SBF with nanosize HAp formations covering most of the available surface, as can be deduced from the evidences gathered by XRD and FTIR (**Fig. 4a-b)**. With the immersion time increasing to 8 h, the individual NPs tended to group in clusters of larger sizes. These features resemble the microstructure of HAp precipitated on pure HAp ceramics after 1 week in SBF **[37]**. This is supported by the gradual intensification of FTIR peaks of HAp seen in the spectra of **67S24C-FD** and **67S24C-CD** samples (**Fig. 4a-b**).

The HAp surface layer continued to develop between 1 and 4 weeks becoming gradually more crystalline as seen in **Fig. 4c, and 6b**. After immersion for 4 weeks, the particles of both **67S24C-CD** and **67S24C-FD** exhibit a dense coverage of crystalline

flakes or plates, but with the same morphological features as those observed in **67S24C-FD** after 8 h. This refinement of the surface morphology is probably due to the local continuous and slowly dissolution/precipitation reactions that occur when the system approaches equilibrium conditions. This nanotextured surface may offer favourable conditions for cell adhesion.

Other reports on rapid glass preparation routes, such as those by Yan *et al.* (a gel calcined at 800 ºC) **[33]** and by Peitl *et al.* (from a glass melt quenching route) **[44]**, indicate the appearance of the phosphate peaks at around 560–600 cm^{-1} in the FTIR spectra only after 24 h and 20 h of immersion in SBF, respectively – much longer periods than 4 h reported here. Furthermore, these and many other publications do not show XRD data or SEM images of the microstructures hindering any well supported comparison with our bioglasses concerning the biomoneralization extents after a given immersion time period.

4. Conclusions

Quaternary (67Si–24Ca–5Na–4P) glass powders were successfully synthesised by sol-gel technique using both conventional drying (**67S24C-CD)** and an innovative fast drying (**67S24C-FD**) process. The two samples were thermally stabilised at 550 ºC and characterised for the physical properties, and assess their biomineralisation capabilities upon immersion in SBF. The relatively high Ca content favoured the depolymerisation of the silica matrix resulting in a network connectivity value of ~3. Although the network structures of the two samples were very similar, the degree of polymerisation of the rapidly dried sample **67S24C-FD** was slightly lower than that of conventional dried sample **67S24C-CD**. Both stabilised glasses contained poorly crystalline HAp. Crystalline silica was also identified as secondary phase in the **67S24C-CD** sample. Although both samples

exhibited good biomineralisation responses upon immersion in SBF, the rapidly dried one (**67S24C-FD**) showed an improved growth of crystalline HAp especially along the earlier periods of contact with SBF. This study confirms the superiority of the FD rapid drying method in terms of the overall performance of the sol-gel derived bioactive glasses.

Acknowledgments

R.C. Pullar wishes to thank the FCT Grant IF/00681/2015 for supporting this work. This work was developed in the scope of the project CICECO−Aveiro Institute of Materials (Ref. FCT UID /CTM /50011/2013), financed by national funds through the FCT/MEC and when applicable co-financed by FEDER under the PT2020 Partnership Agreement.

References

[1] A. Balamurugan, G. Sockalingum, J. Michel, J. Fauré, V. Banchet, L. Wortham, et al., Synthesis and characterisation of sol gel derived bioactive glass for biomedical applications, Mater. Lett. 60 (2006) 3752–3757. doi:10.1016/j.matlet.2006.03.102.

[2] L.C. Klein, Sol-gel technology for thin films, fibers, preforms, electronics, and specialty shapes, Noyes Publications, New Jersey, 1988.

[3] C.S. Chai, K.A. Gross, B. Ben-Nissan, Critical ageing of hydroxyapatite sol-gel solutions., Biomaterials. 19 (1998) 2291–2296. doi:10.1016/S0142-9612(98)90138-7.

[4] K. Zheng, A. Solodovnyk, W. Li, O.-M. Goudouri, C. Stahli, S.N. Nazhat, et al., Aging Time and Temperature Effects on the Structure and Bioactivity of Gel-Derived 45S5 Glass-Ceramics, J. Am. Ceram. Soc. 38 (2015) 30–38. doi:10.1111/jace.13258.

[5] D.M. Liu, T. Troczynski, W.J. Tseng, Aging effect on the phase evolution of water-based sol-gel hydroxyapatite, Biomaterials. 23 (2002) 1227–1236. doi:10.1016/S0142-9612(01)00242-3.

[6] B.A.E. Ben-Arfa, I.M.M. Salvado, J.M.F. Ferreira, R.C. Pullar, Novel route for rapid sol-gel synthesis of hydroxyapatite, avoiding ageing and using fast drying with a 50-fold to 200-fold reduction in process time, Mater. Sci. Eng. C. 70 (2017) 796–804. doi:10.1016/j.msec.2016.09.054.

[7] B.A.E. Ben-Arfa, H.R. Fernandes, I.M.M. Salvado, J.M.F. Ferreira, R.C. Pullar, Synthesis and bioactivity assessment of high silica content quaternary sol-gel glasses with Ca:P ratios of 1.5 and 1.67, J. Biomed. Mater. Res. Part A. 106A (2018) 510–520. doi:10.1002/jbm.a.36239.

[8] L.L. Hench, The story of Bioglass, J. Mater. Sci. Mater. Med. 17 (2006) 967–978. doi:10.1007/s10856-006-0432-z.

[9] I. Kinnunen, K. Aitasalo, M. Po, Reconstruction of orbital floor fractures using bioactive glass, J. Cranio-Maxillofacial Surg. 28 (2000) 229–234. doi:10.1054/jcms.2000.0140.

[10] P. Saravanapavan, J.R. Jones, R.S. Pryce, L.L. Hench, Bioactivity of gel – glass

powders in the CaO-SiO 2 system : A comparison with ternary (CaO-P2O5-SiO2) and quaternary glasses (SiO2-CaO-P2O5-Na2O), J. Biomed. Mater. Res. Part A. (2003) 17–19.

[11] J.R. Jones Review of bioactive glass: From Hench to hybrids, Acta Biomater. 9 (2013) 4457-4486. doi: 0.1016/j.actbio.2012.08.023.

[12] A. Pedone, T. Charpentier, G. Malavasi, M.C. Menziani, V.G. Campi, D. Chimica, New Insights into the Atomic Structure of 45S5 Bioglass by Means of Solid-State NMR Spectroscopy and Accurate First-Principles Simulations, Chem. Mater. 22 (2010) 5644–5652. doi:10.1021/cm102089c.

[13] M. Edén, P. Sundberg, C. Stalhandske, The split network analysis for exploring composition – structure correlations in multi-component glasses : II . Multinuclear NMR studies of alumino-borosilicates and glass-wool fi bers, J. Non. Cryst. Solids. 357 (2011) 1587–1594. doi:10.1016/j.jnoncrysol.2010.11.101.

[14] S. Lin, C. Ionescu, K.J. Pike, E. Smith, J.R. Jones, Nanostructure evolution and calcium distribution in sol – gel derived bioactive glass, J. Mater. Chem. 19 (2009) 1276–1282. doi:10.1039/b814292k.

[15] B.A.E. Ben-arfa, I.M.M. Salvado, J.M.F. Ferreira, R.C. Pullar, The Influence of Cu 2 + and Mn 2 + Ions on the Structure and Crystallization of Diopside – Calcium Pyrophosphate Bioglasses, Int. J. Appl. Glas. Sci. 354 (2016) 345–354. doi:10.1111/ijag.12201.

[16] B.A.E. Ben-Arfa, I.M.M. Salvado, J.M.F. Ferreira, R.C. Pullar, The effect of functional ions (Y3+, F-, Ti4+) on the structure, sintering and crystallization of diopside-calcium pyrophosphate bioglasses, J. Non. Cryst. Solids. 443 (2016) 162–171. doi:10.1016/j.jnoncrysol.2016.04.028.

[17] A. Patel, J.C. Knowles, Investigation of silica-iron-phosphate glasses for tissue engineering, J. Mater. Sci. Mater. Med. 17 (2006) 937–944. doi:10.1007/s10856-006-0183-x.

[18] F. Foroutan, N.J. Walters, G.J. Owens, N.J. Mordan, H. Kim, N.H. De Leeuw, et al., applications Sol – gel synthesis of quaternary (P 2 O 5) 55 – (CaO) 25 – (Na 2 O) (20 − x), Biomed. Mater. (n.d.) 45025. doi:10.1088/1748-6041/10/4/045025.

[19] G. Kaur, G. Pickrell, N. Sriranganathan, V. Kumar, D. Homa, Review and the state of the art: Sol-gel and melt quenched bioactive glasses for tissue engineering, J. Biomed. Mater. Res. - Part B Appl. Biomater. 104 (2016) 1248–1275. doi:10.1002/jbm.b.33443.

[20] R.J. Angel, C.S.J. Shaw, G. V. Gibbs, Compression mechanisms of coesite, Phys. Chem. Miner. 30 (2003) 167–176. doi:10.1007/s00269-003-0303-9.

[21] C. Mochales, R.M. Wilson, S.E.P. Dowker, M.P. Ginebra, Dry mechanosynthesis of nanocrystalline calcium deficient hydroxyapatite: Structural characterisation, J. Alloys Compd. 509 (2011) 7389–7394. doi:10.1016/j.jallcom.2011.04.033.

[22] A.L.B. Maçon, T.B. Kim, E.M. Valliant, K. Goetschius, R.K. Brow, D.E. Day, et al., A unified in vitro evaluation for apatite-forming ability of bioactive glasses and their variants, J. Mater. Sci. Mater. Med. 26 (2015) 1–10. doi:10.1007/s10856-015-5403-9.

[23] A. Oyane, H.-M. Kim, T. Furuya, T. Kokubo, T. Miyazaki, T. Nakamura, Preparation and assessment of revised simulated body fluids, J Biomed Mater Res. 65 (2003) 188–195. doi:10.1002/jbm.a.10482.

[24] G. Poologasundarampillai, D. Wang, S. Li, J. Nakamura, R. Bradley, P.D. Lee, et al., Cotton-wool-like bioactive glasses for bone regeneration, Acta Biomater. 10 (2014) 3733–3746. doi:10.1016/j.actbio.2014.05.020.

[25] Z. Lin, J.R. Jones, J. V Hanna, M. Smith, A multinuclear solid state NMR spectroscopic study of the structural evolution of disordered calcium silicate sol-gel biomaterials, Phys. Chem. Chem. Phys. 17 (2015) 2540–2549. doi:10.1039/c4cp04492d.

[26] B.A.E. Ben-Arfa, I.M. Miranda Salvado, J.M.F. Ferreira, R.C. Pullar, A hundred times faster: Novel, rapid sol-gel synthesis of bio-glass nanopowders (Si-Na-Ca-P system, Ca:P = 1.67) without aging, Int. J. Appl. Glas. Sci. 8 (2017) 337–343. doi:10.1111/ijag.12255.

[27] M. Araújo, M. Miola, G. Baldi, J. Perez, E. Verné, Bioactive glasses with low Ca/P ratio and enhanced bioactivity, Materials (Basel). 9 (2016). doi:10.3390/ma9040226.

[28] P. Innocenzi, Infrared spectroscopy of sol-gel derived silica-based films: A spectra-

microstructure overview, J. Non. Cryst. Solids. 316 (2003) 309–319. doi:10.1016/S0022-3093(02)01637-X.

[29] H. Aguiar, J. Serra, P. González, B. León, Structural study of sol-gel silicate glasses by IR and Raman spectroscopies, J. Non. Cryst. Solids. 355 (2009) 475–480. doi:10.1016/j.jnoncrysol.2009.01.010.

[30] L. Stoch, M. Środa, Infrared spectroscopy in the investigation of oxide glasses structure, J. Mol. Struct. 511–512 (1999) 77–84. doi:10.1016/S0022-2860(99)00146-5.

[31] H. Aguiar, J. Serra, P. González, B. León, Structural study of sol-gel silicate glasses by IR and Raman spectroscopies, J. Non. Cryst. Solids. 355 (2009) 475–480. doi:10.1016/j.jnoncrysol.2009.01.010.

[32] M. Taherian, R. Rojaee, M. Fathi, M. Tamizifar, Effect of different sol-gel synthesis processes on microstructural and morphological characteristics of hydroxyapatite-bioactive glass composite nanopowders, J. Adv. Ceram. 3 (2014) 207–214. doi:10.1007/s40145-014-0111-3.

[33] A. Ignatius, M. Ohnmacht, L.E. Claes, J. Kreidler, F. Palm, A Composite Polymer / Tricalcium Phosphate Membrane for Guided Bone Regeneration in Maxillofacial Surgery, J Biomed Mater Res. 58 (2001) 564–569. doi:10.1002/jbm.1055.

[34] A. Ślósarczyk, Z. Paszkiewicz, C. Paluszkiewicz, FTIR and XRD evaluation of carbonated hydroxyapatite powders synthesized by wet methods, J. Mol. Struct. 744–747 (2005) 657–661. doi:10.1016/j.molstruc.2004.11.078.

[35] G. Lefèvre, T. Preo, J. Lützenkirchen, Attenuated Total Reflection – Infrared Spectroscopy Applied to the Study of Mineral – Aqueous Electrolyte Solution Interfaces : A General Overview and a Case Study, Infrared Spectrosc. Intech. (2011) 979-953-307-362–9.

[36] A. Beganskiene, V. Sirutkaitis, M. Kurtinaitiene, R. Juskenas, A. Kareiva, FTIR, TEM and NMR Iinvestigations of Stöber Silica Nanoparticles, Mater. Sci. 10 (2004) 287–290. doi:10.1016/j.jnoncrysol.2012.11.006.

[37] C. Piccirillo, R.C. Pullar, E. Costa, A. Santos-silva, M.M.E. Pintado, P.M.L. Castro, Hydroxyapatite-based materials of marine origin : A bioactivity and sintering study,

Mater. Sci. Eng. C. 51 (2015) 309–315. doi:10.1016/j.msec.2015.03.020.

[38] E. Landi, G. Celotti, G. Logroscino, A. Tampieri, Carbonated hydroxyapatite as bone substitute, J. Eur. Ceram. Soc. 23 (2003) 2931–2937. doi:10.1016/S0955-2219(03)00304-2.

[39] R.F.S. Lenza, W.L. Vasconcelos, Structural evolution of silica sols modified with formamide, Mater. Res. 4 (2001) 175–179. doi:10.1590/S1516-14392001000300006.

[40] R.F.S. Lenza, W.L. Vasconcelos, Preparation of silica by sol-gel method using formamide, Mater. Res. 4 (2001) 189–194. doi:10.1590/S1516-14392001000300008.

[41] D. Scarano, a. Zecchina, S. Bordiga, F. Geobaldo, G. Spoto, G. Petrini, et al., Fourier-transform infrared and Raman spectra of pure and Al-, B-, Ti- and Fe-substituted silicalites: stretching-mode region, J. Chem. Soc. Faraday Trans. 89 (1993) 4123. doi:10.1039/ft9938904123.

[42] K. Kamiya, A. Oka, H. Nasu, T. Hashimoto, Comparative study of structure of silica gels from different sources, J. Sol-Gel Sci. Technol. 19 (2000) 495–499. doi:10.1023/A:1008720118475.

[43] I. Notingher, J.R. Jones, S. Verrier, I. Bisson, P. Embanga, P. Edwards, et al., Application of FTIR and Raman spectroscopy to characterisation of bioactive materials and living cells, Spectrosc. Int. J. 17 (2003) 275–288. doi:10.1155/2003/893584.

[44] O. Peitl, E.D. Zanotto, L.L. Hench, Highly bioactive P2O5-Na2O-CaO-SiO2 glass-ceramics, Non-Crystalline Solids. 292 (2001) 115–126. doi:10.1016/S0022-3093(01)00822-5.

Figure Captions

Fig. 1 Flow chart scheme of the sol gel synthesis.

Fig. 2 Deconvoluted 29Si-NMR spectra for stabilised glass powders obtained through a) fast drying (FD), and b) conventional drying (CD) routes.

Fig. 3 Structural and morphological features of the 67S24C-FD and 67S24C-CD stabilised glass powders before immersion in SBF: (a) XRD patterns; (b) FTIR spectra; (c) and (d) SEM micrographs.

Fig. 4 Structural evolutions undergone by the FD and CD stabilised glass powders after immersion in SBF for different periods of time (4 h, and 4 w) assessed by: (a); XRD; (b) FTIR.

Fig. 5 Evolution of solution pH with immersion time in SBF for the 67S24C–FD and 67S24C–CD samples

Fig. 6 SEM images for 67S24C-FD and 67S24C-CD glass powders after immersion in SBF for (a) 4 h, (b) 8 h, (c) 1w, and (d) 4w.

Tables

Table 1. Composition, drying schedules and sample codes.

Composition (mol%)	***Drying schedule***	***Sample code***
$67SiO_2 - 5Na_2O - 24CaO - 4P_2O_5$ (67Si – 10Na – 24Ca – 8P)	Conventional drying **(CD)**	**67S24C–CD**
	Rotary evaporator (**FD)**	**67S24C–FD**

Table 2. Physical properties (density, particle size, and specific surface area) of **67S24C–CD** and **67S24C–FD** glasses.

Sample code	Density (g/cm^3)	Particle size d_{50} (μm)	BET SSA m^2/g
67S24C–CD	2.3 ± 0.03	34±0.34	99.5
67S24C–FD	2.5 ± 0.03	16±0.24	68.1

Table 3. Q^n (Si) distribution for **67S24C–CD** and **67S24C–FD** glasses obtained by NMR deconvolution, and calculated degrees of condensation (D_c) and network connectivity (N_c).

Sample code	Q^n								D_c (%)	N_c from ^{29}Si MAS NMR
	Q1		Q^2		Q^3		Q^4			
	Peak position (ppm)	*Integral %*	*Peak position (ppm)*	*Integral %*	*Peak position (ppm)*	*Integral %*	*Peak position (ppm)*	*Integral %*		
67S24C–FD	–86.5	11.3	–94.4	29.0	–100.2	9.4	–110.4	50.3	71.8	3.0
67S24C–CD	–88.2	9.8	–96.4	19.4	–100.7	8.5	–110.3	62.3	78.4	3.2

Figure Captions

Fig. 1 Flow chart scheme of the sol gel synthesis.

Fig. 2 Deconvoluted 29Si-NMR spectra for stabilised glass powders obtained through (a) fast drying (FD), and (b) conventional drying (CD) routes.

Fig. 3 Structural and morphological features of the 67S24C-FD and 67S24C-CD stabilised glass powders before immersion in SBF: (a) XRD patterns; (b) FTIR spectra; (c) and (d) SEM micrographs.

Fig. 4 Structural evolutions undergone by the FD and CD stabilised glass powders after immersion in SBF for different periods of time (4 h, and 4 w) assessed by: (a); XRD; (b) FTIR.

Fig. 5 Evolution of solution pH with immersion time in SBF for the 67S24C–FD and 67S24C–CD samples

Fig. 6 Fig. 6 SEM images for 67S24C-FD and 67S24C-CD glass powders after immersion in SBF for (a) 4 h, (b) 8 h, (c) 1w, and (d) 4w.

Figures

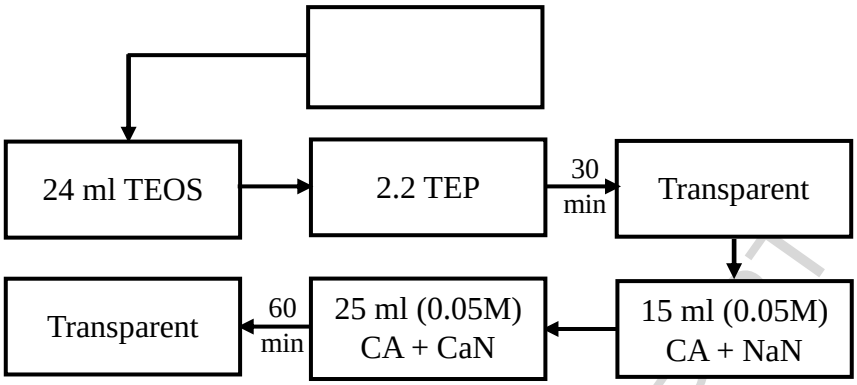

Fig. 1 Flow chart scheme of the sol gel synthesis.

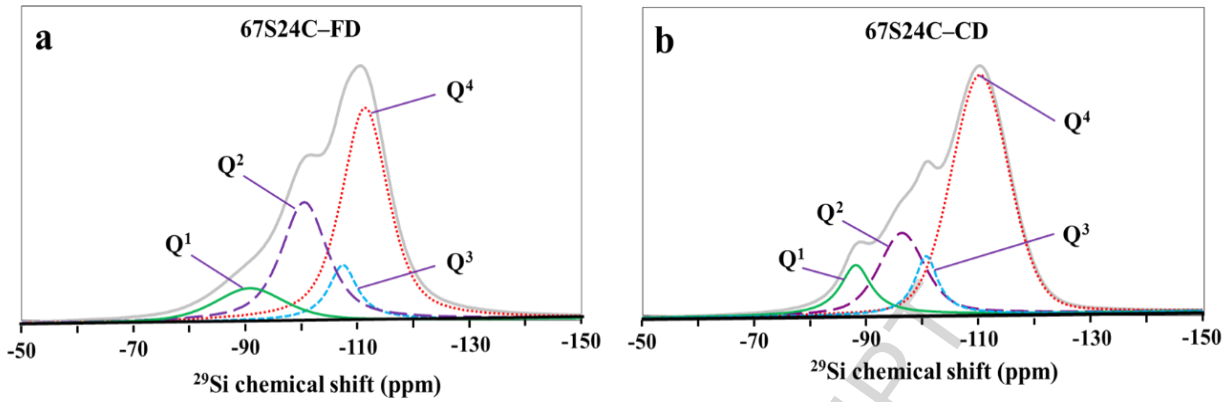

Fig. 2 Deconvoluted ^{29}Si-NMR spectra for stabilised glass powders obtained through a) fast drying (FD) and b) conventional drying (CD) routes.

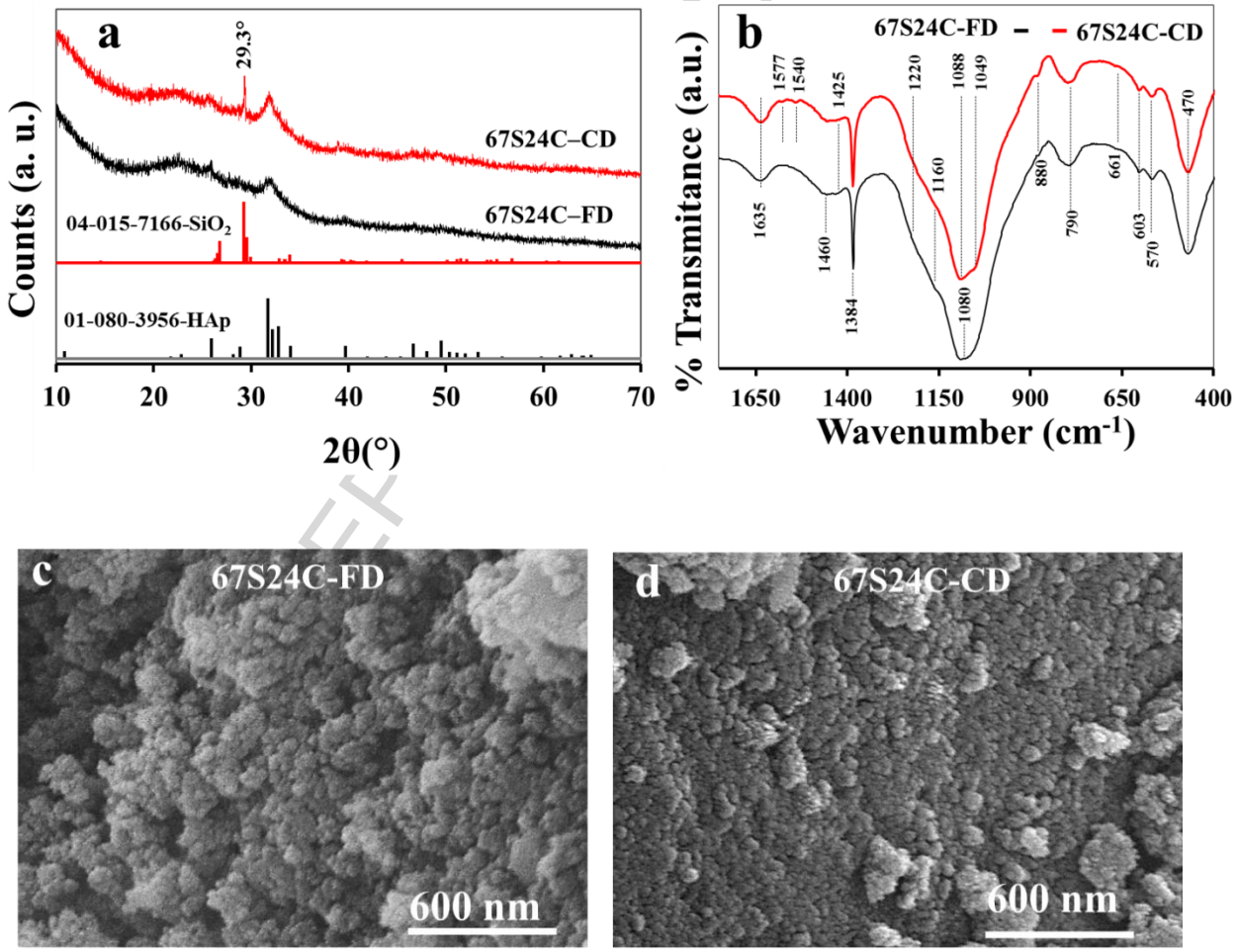

Fig. 3 Structural and morphological features of the 67S24C-FD and 67S24C-CD stabilised glass powders before immersion in SBF: (a) XRD patterns; (b) FTIR spectra; (c) and (d) SEM micrographs.

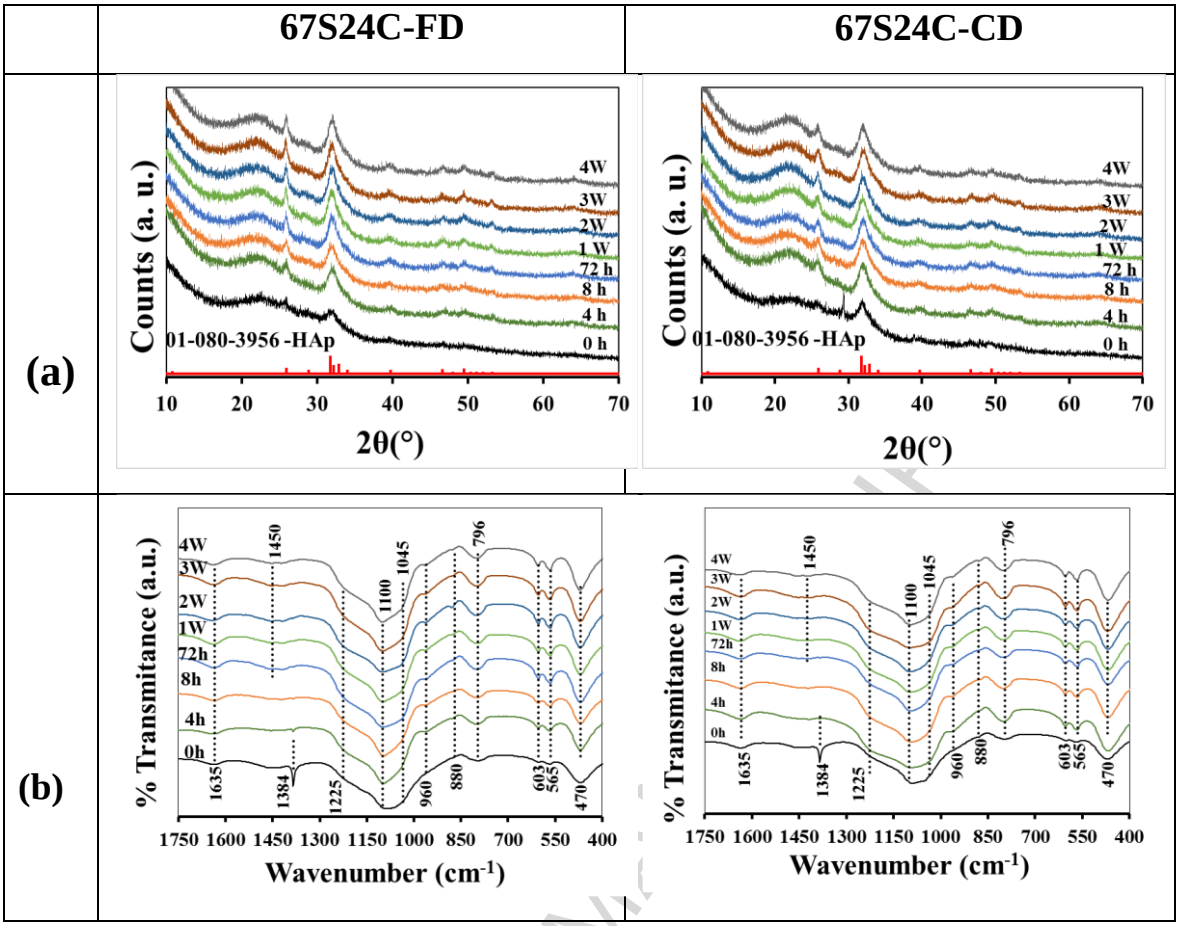

Fig. 4 Structural evolutions undergone by the FD and CD stabilised glass powders after immersion in SBF for different periods of time (4 h, and 4 w) assessed by: (a); XRD; (b) FTIR.

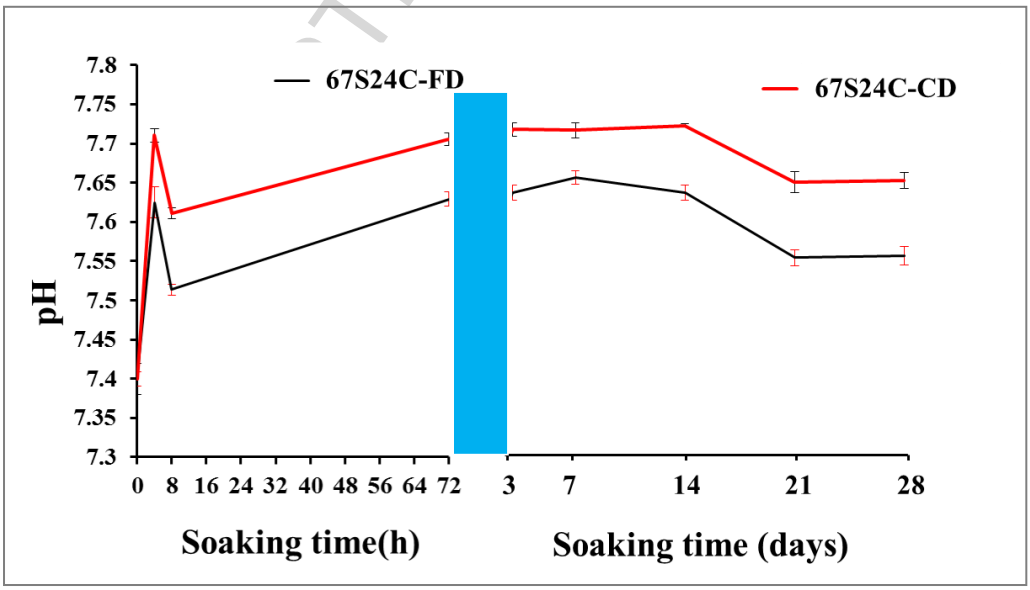

Fig. 5 Evolution of solution pH with immersion time in SBF for the 67S24C–FD and 67S24C–CD samples

	67S24C-FD	67S24C-CD
(a)	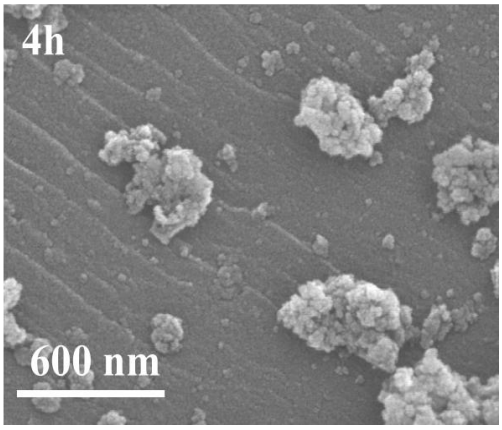	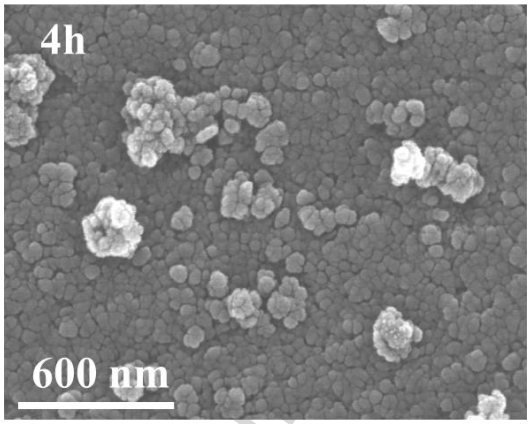
(b)	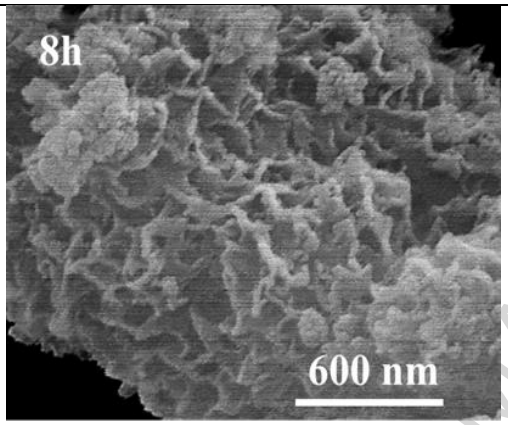	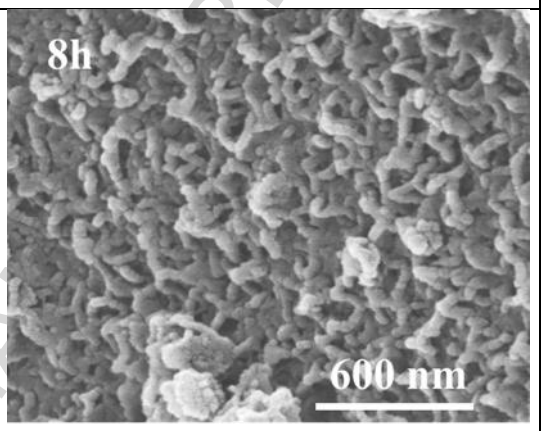
(c)	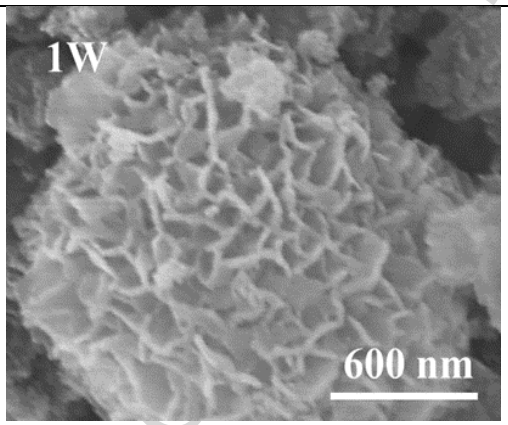	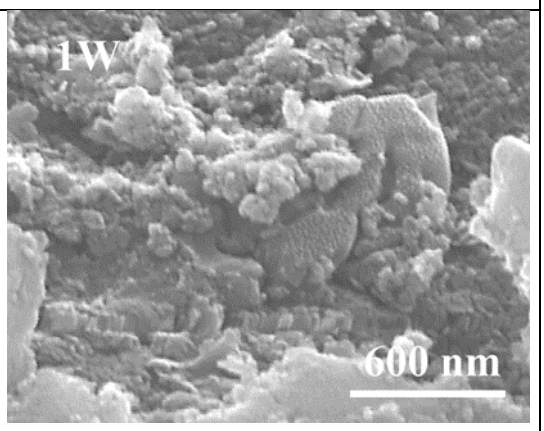
(d)	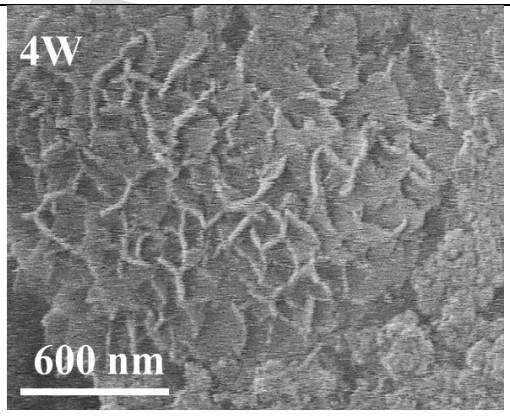	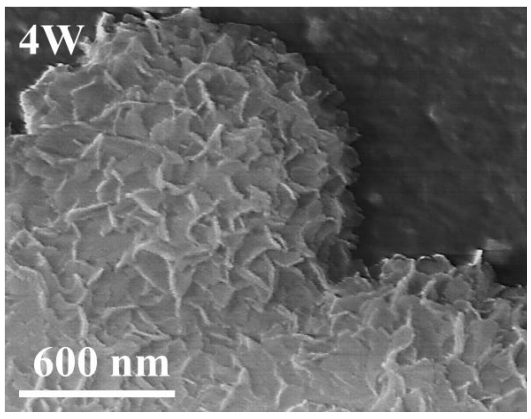

Fig. 6 SEM images for 67S24C–FD and 67S24C–CD glass powders after immersion in SBF for (a) 4 h, (b) 8 h, (c) 1w, and (d) 4w.

Graphical Abstract

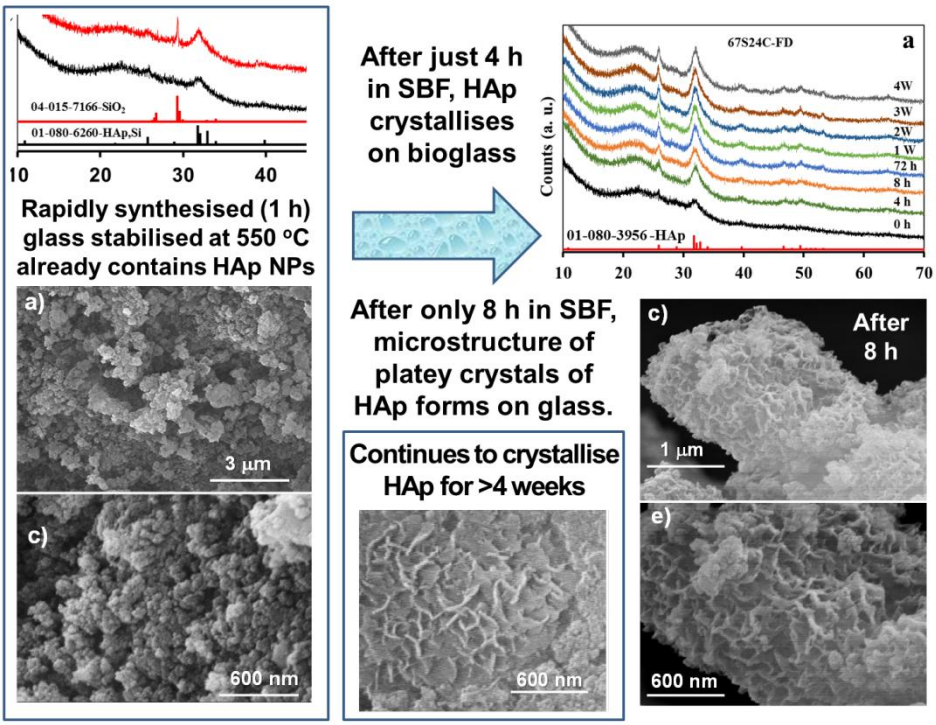

Enhanced bioactivity of a rapidly-dried sol-gel derived quaternary bioglass

Basam A. E. Ben-Arfa, Isabel M. Miranda Salvado*, José M. F. Ferreira and Robert C. Pullar*

Department of Materials and Ceramic Engineering / CICECO – Aveiro Institute of Materials, University of Aveiro, 3810-193 Aveiro, Portugal

Highlights

- Novel quaternary (67Si-24Ca-10Na-8P) glass powders made by sol-gel synthesis.
- Compared slow conventional drying (CD) and an innovative fast drying (FD) process (200 times quicker).
- High Ca levels produced a less polymerised, more open, network structure with improved bioactivity in SBF.
- Both showed very similar silica network structures, but FD had a slightly lower degree of polymerisation than CD.
- The CD glass exhibited an unwanted secondary crystalline silica phase.
- Both glasses showed excellent biomineralisation in SBF, with evidence of HAp formation in FD after 4 h, while CD needed between 8 h and 1 week.